J Mater Sci: Mater Med (2007) 18:1009–1016
DOI 10.1007/s10856-006-0114-x

Calcium phosphates formation on $CaTiO_3$ coated titanium

Naofumi Ohtsu · Kenji Sato · Kesami Saito · Katsuhiko Asami · Takao Hanawa

Received: 9 May 2005 / Accepted: 27 January 2006 / Published online: 23 January 2007

Abstract In this study, performance of calcium phosphate formation of $CaTiO_3$ coating film on Ti in Hanks' balanced saline solution (HBSS) was investigated. $CaTiO_3$ thin films with a thickness of 50 nm were deposited on Ti using radiofrequency (RF) magnetron sputtering. The temperature of Ti substrate was adjusted to room temperature (RT) and 873 K. Thereafter, the specimens deposited at RT were annealed at 873 K in air for 7.2 ks. The films were characterized by grazing incident angle X-ray diffractometry (GI-XRD) and X-ray photoelectron spectroscopy (XPS). After immersion in HBSS for 60 d, on $CaTiO_3$ coated Ti, the formation of hydroxyapatite (HAP) was observed. Furthermore, HAP layer formed was thicker on the specimen on which $CaTiO_3$ film was deposited at RT and annealed than that prepared at 873 K. The major difference between both specimens was the chemical properties of the outermost surface. In summary, $CaTiO_3$ thin film deposited at RT and followed by annealing at 873 K for 7.2 ks in air enhances calcium phosphate formation ability on Ti.

Introduction

Titanium and its alloys have been widely used as biomedical and dental materials because of their excellent biocompatibility [1] and good mechanical properties [2]. However, it takes long time for these materials to bond directly to living bone. Improvement of bone-conductivity of these materials is demanded from biomedical field such as orthopedics and dentistry. In order to enhance the ability of these materials, various surface modification techniques have been attempted. Most of these techniques are physical coating processes with foreign calcium phosphate ceramic materials with high bone-conductivity, such as hydroxyapatite (HAP; $Ca_{10}(PO_4)_6(OH)_2$) and tricalcium phosphate (TCP; $Ca_3(PO_4)_2$). Ceramic coatings due to various deposition techniques, e.g. electrophoretic deposition [3], radiofrequency sputtering [4] and pulsed laser deposition [5], are investigated, and HAP coating with plasma spraying on Ti practically used for dental implants. However, various problems with HAP spray-coated Ti are pointed out by dentists. In particular, fragility of the coated HAP film itself and poor bonding strength between the film and substrate material are serious problems because they result in cracking of the coated film and at the interface during the clinical service [6]. Also, dissolution of the film during implantation is a serious problem because abrupt increase of Ca concentration in living body may induces inflammation.

Recently, bone-conductivity of Ti using implantation of Ca ions at 18 kV is accelerated [7]. It was also reported that the implanted Ca forms unequilibrium $CaTiO_3$ in the modified surface and it promotes the formation of calcium phosphates in the living body [8, 9]. Therefore, it is expected that the bone-conductivity of Ti surface will be enhanced by coating with such a $CaTiO_3$ film. One of the simplest methods to coat $CaTiO_3$ thin layer to Ti-base materials will be the sputter deposition of $CaTiO_3$. On the other hand, the

N. Ohtsu (✉) · K. Sato · K. Saito · K. Asami
Institute for Material Research, Tohoku University, 2-1-1 Katahira, Aoba-ku, Sendai 980-8577 Miyagi, Japan
e-mail: nohtsu@imr.edu

N. Ohtsu · T. Hanawa
Institute of Biomaterials and Bioengineering, Tokyo Medical and Dental University, Tokyo 101-0062, Japan

minimum thickness of the $CaTiO_3$ film for the formation of calcium phosphates will be about the same with the depth of the modified surface by Ca-ions implantation. It is known that the modified depth by Ca^+ implantation to Ti at 18 kV is about 30 nm, which is about 1/1000 compared with that of the HAP film coated with plasma splaying. Generally, mechanical properties of thin film are improved by decreasing its thickness because of dispersion of stress. Consequently, surface modification by coating with $CaTiO_3$ thin film would be better alternative of a thick HAP coating.

In this study, performance of calcium phosphate formation on $CaTiO_3$ thin film deposited with radio-frequency (RF) magnetron sputtering was investigated by immersion in simulated body fluids (SBF). In general, materials which form calcium phosphates rapidly by immersion in SBF have a good bone-conductivity. In addition, we also discussed the $CaTiO_3$ film properties required to form calcium phosphate efficiently on the basis of the characterization of $CaTiO_3$ film.

Experimental procedure

Deposition of $CaTiO_3$ film on Ti

Commercially available pure Ti (cpTi) grade 2 (ISO 5832-2) with a disk shape (ϕ8 mm × t1 mm) was mechanically polished with SiC paper (#1500) to obtain a rough surface. $CaTiO_3$ films were deposited on cpTi substrate using RF magnetron sputtering with $CaTiO_3$ target in Ar gas flow. The background pressure of deposition chamber was about 10^{-7} Pa. The thickness of deposited films was estimated from the monitored sputtering rate of $CaTiO_3$ film and adjusted to about 50 nm. Sputtering power was fixed to 200 W. The $CaTiO_3$ thin film with low crystallinity dissolves rapidly in the SBF [10]. Therefore, we conducted two types of heat treatments to the film to increase the crystallinity and to prevent an abrupt dissolution: (1) the specimens were prepared at room temperature (RT), followed by annealing at 873 K for 7.2 ks in air (H1), and (2) the temperature of substrate was adjusted to 873 K during deposition (H2). For comparison, some specimens were prepared at RT but did not heat-treated. Specimen preparation conditions are summarized in Table 1.

Characterization of the $CaTiO_3$ films

Grazing incident angle X-ray diffractmetry (GI-XRD) was conducted with a step-scanning mode at 0.1 deg/min and a X-ray incident angle of 1 degree against the specimen surface (Rotaflex RU-200B, Rigaku, Japan).

X-ray photoelectron spectroscopy (XPS) was carried out in a pressure of about 10^{-8} Pa. Photoelectrons were excited by Al Kα radiation ($h\nu$ = 1486.6 eV) of a monochromatized X-ray source (SSX-100, Surface Science Inc, USA). In order to correct the electron-energy shift caused by charging effect, Au thin film with about 0.5-nm thickness was deposited on all specimens and all spectra were adjusted by taking the Au $4f_{7/2}$ peak position from the Au thin film as 84.0 eV. The photoionization cross-sections of the Ti $2p_{3/2}$, Ca $2p_{3/2}$ and O 1s peaks relative to that of C 1s peak used for quantification from the integrated intensities were 5.22, 3.35 and 2.93 [11], respectively.

Evaluation of calcium phosphate formation

Hanks' balanced saline solution (HBSS) as a SBF was employed to evaluate the performance of calcium phosphate formation. The ion concentrations of the HBSS and human blood plasma are compared in Table 2. The HBSS was prepared by dissolving reagent-grade $CaCl_2$, KH_2PO_4 3H2O, KCl, NaCl, $MgSO_4$ $7H_2O$, $NaHCO_3$, and Na_2HPO_4 (Nacalai Tesque, Inc) in deionized water (Millipore). Five each specimens prepared at RT, H1 and H2 were immersed in 12.2 mL of the HBSS at 310 K for 30, 45 and 60 d. For comparison, five cpTi, which was polished by SiC paper (#1500), were also immersed. Avoiding Si contamination eluted from the vessels [12], specimens were immersed in the vessels made of perfluoroalkoxy fluoroplastic (Tefron©PFA) and the vessel was completely sealed. The pH value of HBSS was adjusted to

Table 1 Specimen preparation conditions

Symbol	Sputtering conditions			Treatment after deposition
	Sputtering power	Thickness of $CaTiO_3$ film	Temperature of substrate	
RT	200 W	50 nm	Room temperature	No
H1	200 W	50 nm	Room temperature	Keep at 873 K for 7.2 ks. in air
H2	200 W	50 nm	873 K	No

Table 2 Ion concentrations of Hanks' balanced saline solution (HBSS) and human blood plasma

	Concentration (mol l^{-1})	
	HBSS	Blood plasma
Na^+	1.42×10^{-1}	1.42×10^{-1}
K^+	5.81×10^{-3}	5.00×10^{-3}
Mg^+	8.11×10^{-4}	1.50×10^{-3}
Ca^{2+}	1.26×10^{-3}	2.50×10^{-3}
Cl^-	1.45×10^{-1}	1.03×10^{-1}
HPO_4^{2-}	7.78×10^{-4}	1.00×10^{-3}
SO_4^{2-}	8.11×10^{-4}	1.50×10^{-3}
CO_3^{2-}	4.17×10^{-3}	2.7×10^{-2}

7.4 by the addition of dropwise HCl solution twice a week. After the allotted immersion periods, the specimens were retrieved from the HBSS, gently rinsed with distilled water, and dried in a convection oven at 313 K.

The formation of the calcium phosphate was examined using GI-XRD, scanning electron microscopy (SEM) and electron probe micro-analysis (EPMA; JXA-8621MX, JEOL Inc, Japan) equipped with wavelength dispersive X-ray spectrometory (WDS) and energy dispersive X-ray analysis (EDX). The acceleration voltage of SEM and EPMA was 10 kV. The thickness of the calcium phosphate layer was determined by the observation of the cross section view of specimens using SEM when calcium phosphate layer was sufficiently thick.

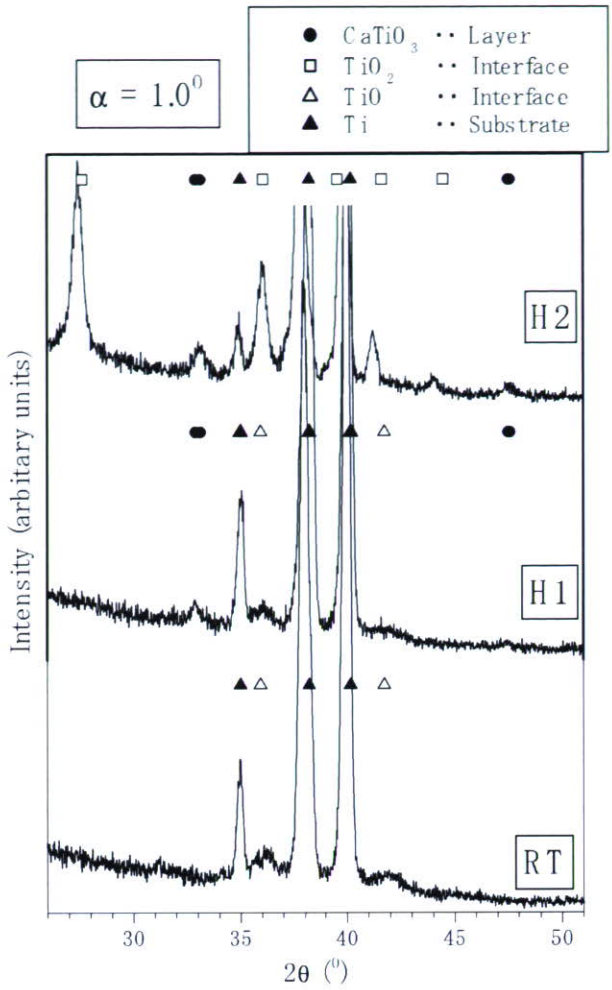

Fig. 1 GI-XRD patterns of RT, H1 and H2 specimens

Results and discussion

Characteristics of $CaTiO_3$ films before immersion

In order to utilize the surface treated cpTi and Ti-alloys in medicine and dentistry, they should be chemically stable and safe for the human body. Thus, one of the important factors for this purpose is the crystallinity of the $CaTiO_3$ film. Figure 1 shows GI-XRD patterns of the specimens before immersion. Since effective depth of GI-XRD analysis is larger than the thickness of the $CaTiO_3$ films, the GI-XRD pattern includes not only peaks from the deposited film but also those from the interface and Ti substrate. Thus, hongquiite-type TiO observed in RT and H2, and rutile type TiO_2 observed in H1 specimen were originated from the layer formed between the film and substrate. These Ti oxide layer should be formed by oxidation at the process of specimen preparation. In RT specimen, the crystallized $CaTiO_3$ was not observed. However, in both H1 and H2 specimens, perovskite-type $CaTiO_3$ was observed. These results indicate that heating at a high temperature such as 873 K is needed for the deposited $CaTiO_3$ thin film to crystallize. This crystallization temperature of $CaTiO_3$ film agrees with that of $CaTiO_3$ film prepared by sol–gel method [13].

XPS peaks of Ca 2p, Ti 2p and O 1s obtained from all specimens are shown in Fig. 2. The shape of Ca 2p peaks of RT specimen is almost symmetry, but those of H1 and H2 specimens are asymmetry and spread to higher energy side. This asymmetry is explained by the two pairs of overlapped peaks as shown in Fig. 2(a). These spectra shapes of Ca 2p and Ti 2p are similar to those of $CaTiO_3$ single-crystal [14]. The O 1s peaks of all specimens were deconvoluted into three peaks originated from anhydrous oxide (O^{2-}), hydroxyl group (OH^-) and adsorbed water (H_2O). The results are shown in Fig. 2(c). The inserted values of $\{[O^{2-}]/([OH^-] + [H_2O])\}$ to Fig. 2 are the concentration

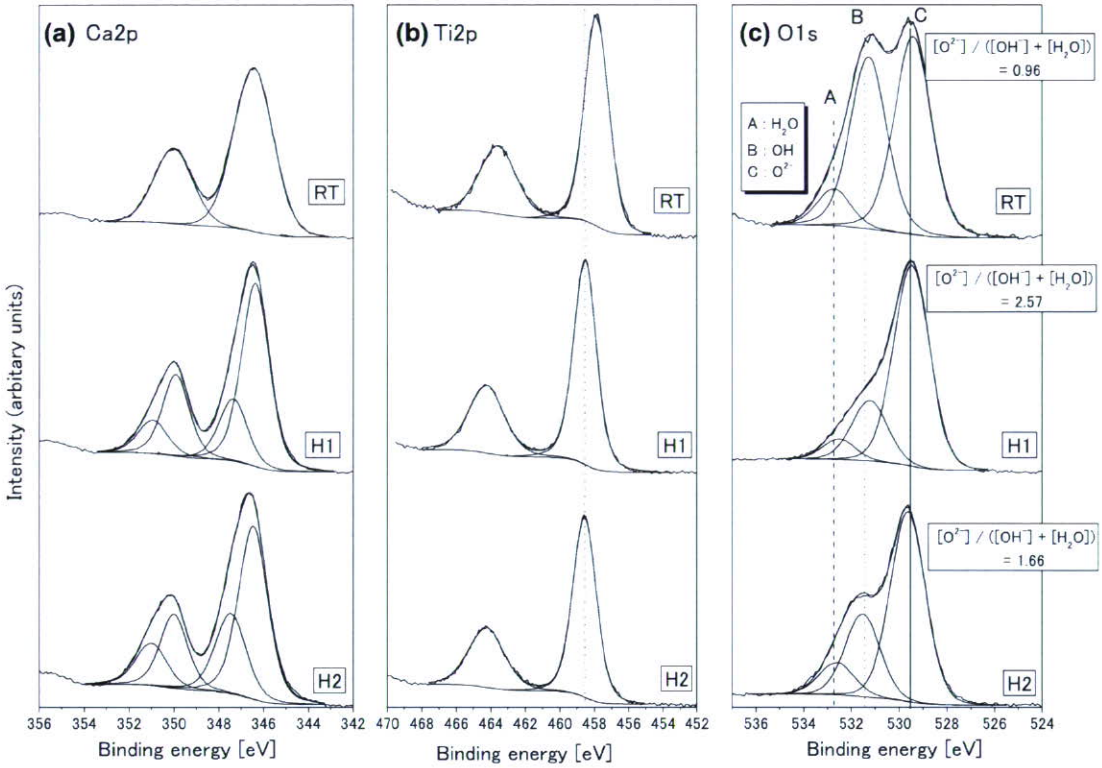

Fig. 2 XPS spectra of Ca 2p, Ti 2p and O 1s obtained from RT, H1 and H2 specimens. Binding energy values were corrected by using Au $4f_{7/2}$ = 84.0 eV. The inserted values of $\{[O^{2-}]/([OH^-] + [H_2O])\}$ are the concentration (at%) ratios calculated from the integrated intensities of O1s peaks

(at%) ratios calculated from the integrated intensities of O1s peaks. The $\{[O^{2-}]/([OH^-] + [H_2O])\}$ concentration (at%) ratios at outermost surface increases in order of RT, H2 and H1 specimens.

The binding energies of Ca $2p_{3/2}$, Ti $2p_{3/2}$, and O 1s energy region peaks are summarized in Table 3. Table 3 also contains the binding energies obtained from $CaTiO_3$, TiO_2 and CaO by a previous study [8]. The binding energies of Ca $2p_{3/2}$ level of all specimens are the almost same as those of $CaTiO_3$. The binding energies of Ti $2p_{3/2}$ level in H1 and H2 specimens are almost the same as that of $CaTiO_3$. The binding energy of Ti $2p_{3/2}$ level in RT specimen is shifted toward to the lower energy than that of $CaTiO_3$. These results indicate that the outermost surfaces in H1 and H2 specimens include the $CaTiO_3$ state. On the other hand, the outermost surface in RT specimen does not include $CaTiO_3$ state and consists of some Ca and Ti oxide states.

The results of quantitative calculation from the integrated intensities are summarized in Table 4. If the outermost surface consists of stoichiometric $CaTiO_3$, the concentration (at%) of Ti should be equal to that of Ca. The concentrations of Ti and Ca are close together in H1 specimen. On the other hand, the concentration of Ti is smaller than that of Ca in H2. These results indicate that the outermost surface in H1 specimen consists of mainly stoichiometric CaTiO, whereas that in H2 specimen include less stoichiometric $CaTiO_3$. In addition, the increase of

Table 3 Binding energies of Ca $2p_{3/2}$, Ti $2p_{3/2}$ and O1s peaks obtained from $CaTiO_3$ thin films, CaO, $CaTiO_3$, and TiO_2 using XPS. Binding energy values were corrected by using Au $4f_{7/2}$ = 84.0 eV

Specimen	Ca $2p_{3/2}$ (eV)	Ti $2p_{3/2}$ (eV)	O 1s $[OH^-]$ (eV)	O1s $[O^{2-}]$ (eV)	Reference
RT	346.8	457.9	531.5	529.5	Present work
H1	346.6	458.6	531.8	529.7	Present work
H2	346.6	458.6	531.6	529.8	Present work
$CaTiO_3$	346.6	458.4	–	–	[8]
TiO_2	–	458.8	–	–	[8]
CaO	347.2	–	–	–	[8]

Table 4 Results of quantitative calculation from the integrated intensities obtained by using XPS. [X] means concentration (at%) of the X

Specimens	$\frac{[Ca]}{([Ca] + [Ti] + [O])}$	$\frac{[Ti]}{([Ca] + [Ti] + [O])}$	$\frac{[O]}{([Ca] + [Ti] + [O])}$	$\frac{[Ti]}{[Ca] + [Ti]}$
RT	0.18	0.11	0.71	0.37
H1	0.17	0.14	0.69	0.45
H2	0.20	0.12	0.68	0.38

concentration (at%) ratio of $\{[O^{2-}]/([OH^-] + [H_2O])\}$ in H1 specimen compared with that in H2 specimen will be resulted from less hydrated surface of H1 specimen.

SEM observation of specimen surface after immersion

Since $CaTiO_3$ film in RT specimen was not crystallized and dissolved abruptly, immersion test was not performed. Figure 3 shows the SEM image of the surfaces of specimens after 30- and 60-d immersions. After immersion for 30 d (Figs. 3(a) and 3(b)), the island-like precipitates were observed on the H1 specimen. After immersion for 60 d (Figs. 3(c) and 3(d)), the surface of specimen was completely covered with precipitate layer and large size precipitates initially observed on the specimens for 30 d disappeared. The precipitate layer contained cracks in Fig. 3(d). The cracks are caused by evacuation of the water in the layer in vacuo. Figure 4 shows the EPMA-EDX spectra of precipitates observed in SEM images after 30- and 60-d immersion (Fig. 3(b) and (d)). Only the peaks from Ca and P were observed, and these precipitates were asssumed as calcium phosphates. The inserted values of [Ca]/[P] correspond to atomic ratios of the calcium phosphate determined by the EPMA-WDS. After immersion for 30 d (Fig. 4(a)), the [Ca]/[P] ratio is slightly smaller than that of HAP {[Ca]/[P] = 1.67}. After immersion for 60 d (Fig. 4(b)), the [Ca]/[P] ratio of the layer is 1.67, and this value is the same as that of HAP. In the initial stage of HAP formation, calcium phosphate with a low {[Ca]/[P]} ratio is formed. The ratio increases with time scale of days and eventually approached to that of HAP. This phenomenon was explained by a faster adsorption of phosphate ions than that of calcium ions, the adsorbed phosphate ions give negative charges at the surface and attract passively charged calcium ions [15]. Our results can be explained by essentially the same mechanism.

Figure 5 shows the SEM image of H2 specimen surface after immersion for 60 d. The surface of H2 specimen was also covered with precipitate layer. Figure 6 shows the EPMA-EDX spectrum of precipitate layer. Not only Ca and P peaks but also Ti peaks are observed in the spectrum. Ti peaks are originated from the $CaTiO_3$ film and Ti substrate because the precipitate layer is thinner than the effective depth of

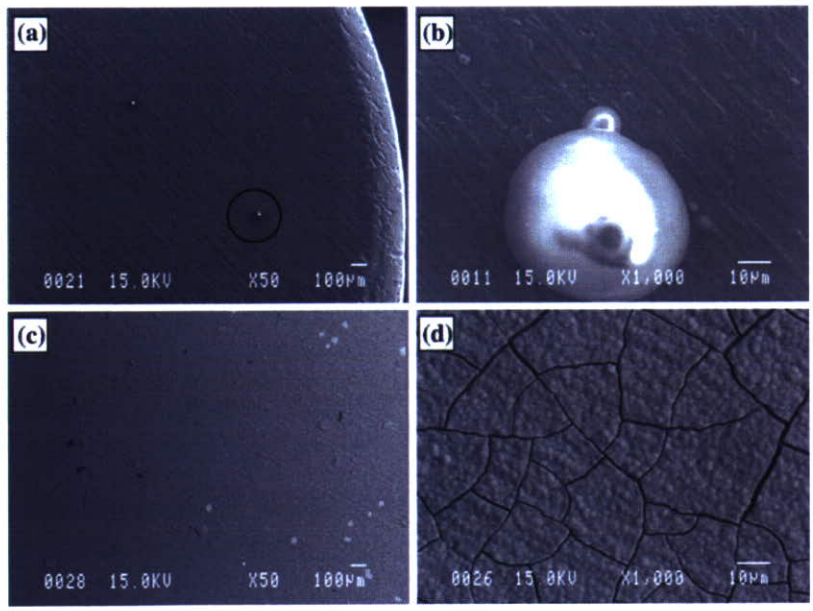

Fig. 3 SEM images of surface of H1 specimen after immersion in HBSS for 30 d (**a** and **b**) and after immersion in HBSS for 60 d (**c** and **d**)

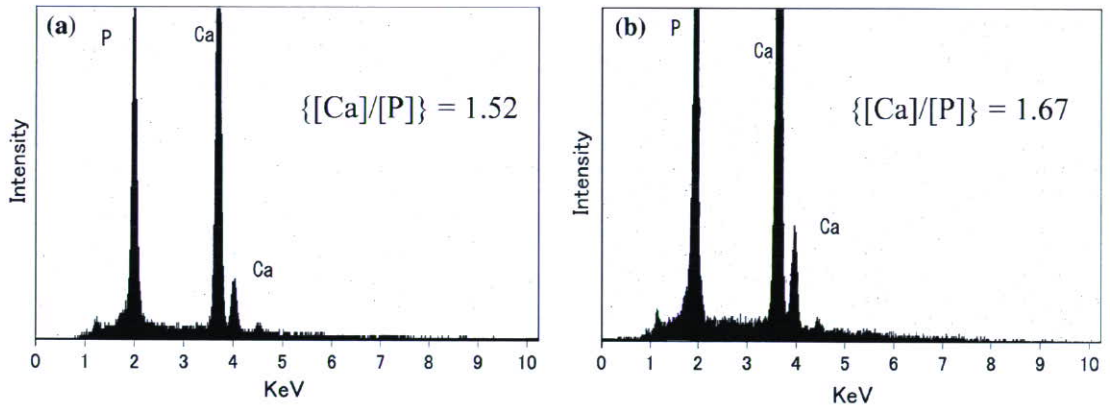

Fig. 4 EPMA-EDX spectra of precipitates of H1 specimen after immersion for 30 d (**a**) and after immersion for 60 d (**b**) in HBSS. Inserted {[Ca]/[P]} values correspond to atomic ratios of the precipitates determined by EPMA-WDS

Fig. 5 SEM images of surface of H2 specimen after immersion in HBSS for 60 d

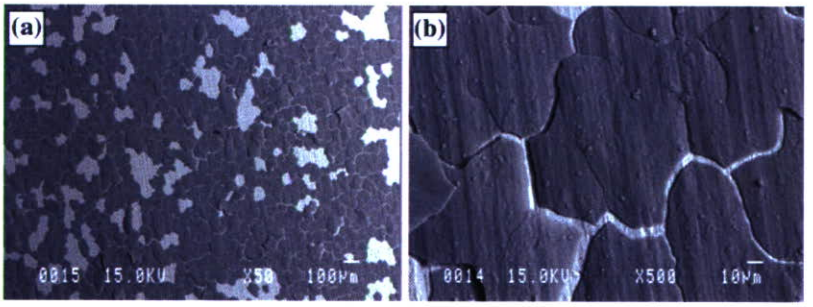

EPMA analysis. Thus, the precipitate layer is identified as calcium phosphates. The atomic ratio of {[Ca]/[P]} determined by the EPMA-WDS is also inserted in Fig. 6. The {[Ca]/[P]} ratio of the layer is slightly larger than that of HAP because Ca signal originated from the $CaTiO_3$ film is also included. The calcium phosphate layer on H2 specimen seems to be much easily peeled off from the substrate than that of H1 specimen. Furthermore, calcium phosphate was observed only on one of two H2 specimens shown in Fig. 5.

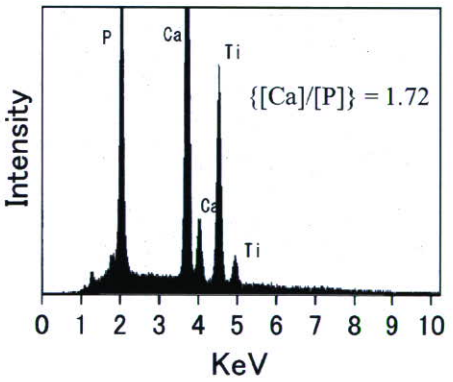

Fig. 6 EPMA-EDX spectrum of precipitates of H2 specimen after immersion for 60 d in HBSS. Inserted {[Ca]/[P]} values correspond to atomic ratios of the precipitates determined by EPMA-WDS

The results of SEM observation of all specimens are summarized in Table 5. The cpTi cannot form any calcium phosphate layer even after immersion for 60 d. Only H1 specimens can form calcium phosphate after immersion for 30, 45 and 60 d. Thus, H1 specimens showed the most stable growth of calcium phosphate layer. These results show that $CaTiO_3$ deposited 50 nm in thickness is enough to enhance the formation of calcium phosphates.

Table 5 The number of specimens formed calcium phosphate after immersion in HBSS

Specimens	30 d	45 d	60 d
cpTi	0/1	0/2	0/2
H1	1/1	2/2	2/2
H2	0/1	0/2	1/2

The number/number of specimen

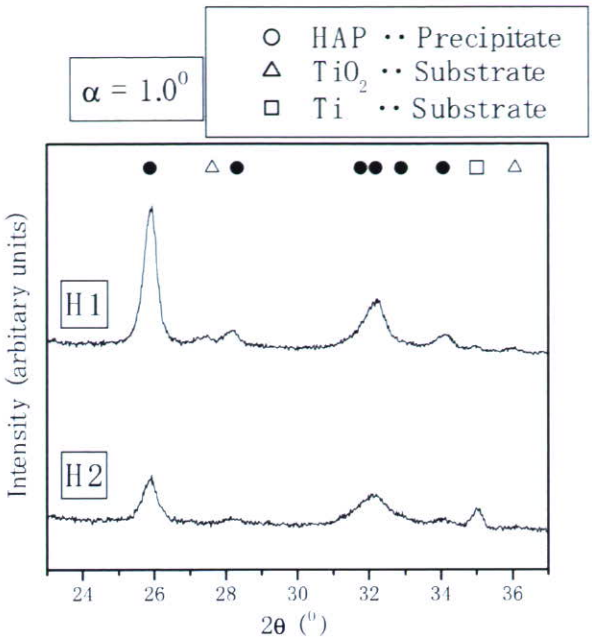

Fig. 7 GI-XRD patterns of the surface of H1 and H2 specimens after immersion in HBSS for 60 d

Figure 7 shows GI-XRD patterns of the surfaces of specimen H1 and H2 specimens after immersion for 60 d. The main peaks are assigned to reflection from HAP. Therefore, the calcium phosphate layers formed after immersion are identified as the HAP layers.

Thickness of calcium phosphate layer after immersion for 60 d

For estimating the thickness of the calcium phosphate layers formed after immersion for 60 d, the cross section of immersed specimens was observed by using SEM. Figure 8 shows the SEM images of cross section of specimens. The calcium phosphate layer on H2 specimen is very easily exfoliated from the substrate. On the other hand, it is rather strongly combined with the substrate on H1 specimen. The thicknesses of calcium phosphate layers determined from the SEM images are summarized in Table 6. The thickness of the calcium phosphate layer formed on the H1 specimen is four times as thick as that on H2 specimen. Thus, the growth rate of calcium phosphate layer on the H1 specimen is also faster than that of the H2 specimen.

Table 6 The thickness of the calcium phosphate layer formed after immersion in HBSS

Specimen	Thickness of calcium phosphate layer (μm)
H1	4.5
H2	1.2

Properties of $CaTiO_3$ film which is required to enhance calcium phosphate formation

Figures 3 and 4 show that the $CaTiO_3$ thin films of both H1 and H2 specimens can enhance the formation of calcium phosphates on Ti substrate. However, Tables 5 and 6 reveal that HAP film growth rates is large on H1 specimen. On both specimens H1 and H2, deposited $CaTiO_3$ is crystallized to perovskite-type $CaTiO_3$ and the compositions are similar. Differences are concentration of [OH] and [Ca]/[Ti] rate at the outermost surface of the deposited film.

Dissolution of Ca from the surface of materials is one of the important events for calcium phosphate formation in SBF. We consider that chemical stability at the outermost surface concern with the degradability of the film. We also attribute the high dissolution rate of Ca in H2 specimen than that in H1 specimen to the difference in the chemical stability of the outermost surface. The difference in the performance of calcium phosphate formation in H1 and H2 specimens may be caused by the difference in dissolution behavior of the outermost surface of the modified $CaTiO_3$ film deposited on Ti. However, more investigation in detail, e.g. determination of Ca amount dissolved into HBSS, is necessary to clarify this idea.

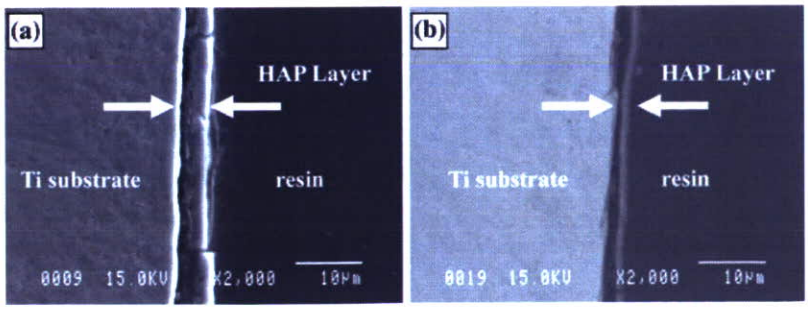

Fig. 8 SEM images of the cross section of: (**a**) H1 specimen and (**b**) H2 specimen after immersion in HBSS for 60 d

Summary

Deposition of $CaTiO_3$ at room temperature followed by annealing at 873 K in air or deposition at 873 K in vacuo could prepare the crystallized pervskite-type $CaTiO_3$ film on Ti. The outermost surfaces in both films were composed of $CaTiO_3$, whereas extent of convolution of hydroxides and other species than $CaTiO_3$ is high on the specimen deposited at 873 K and exposed to air.

After immersion in HBSS, formation of calcium phosphate was observed on $CaTiO_3$ film in both the $CaTiO_3$ film annealed in air and the $CaTiO_3$ film deposited at 873 K. The {[Ca]/[P]} ratio of the calcium phosphate formed on $CaTiO_3$ film at the initial stage is slightly smaller than that of hydroxyapatite. The ratios increased with immersion time and finally reached that of hydroxyapatite. In addition, when calcium phosphate layer was sufficiently thick, it was crystallized to hydroxyapatite. These results indicate that crystallized $CaTiO_3$ film with thickness of 50 nm can enhance the calcium phosphate formation. However, growth rate of the calcium phosphate layer is high on the specimen where the $CaTiO_3$ film was annealed in air in comparison with $CaTiO_3$ film deposited at 873 K. Therefore, in order to enhance the calcium phosphate formation efficiently, $CaTiO_3$ film should be modified by annealing in air rather than deposition on heated substrate in vacuo.

Acknowledgment The authors thank Mr. Yoshihiro Murakami for operating the EPMA.

References

1. A. YAMAMOTO, R. HONMA and M. SUMITA, *J. Biomed. Mater. Res.* **39** (1998) 331
2. M. PAPAKYRIACOU, H. MAYER, C. PYPEN, H. PLENK Jr and S. STANZ-TSCHEGG, *Int. J. Fatigue* **22** (2000) 873
3. K. YaMashita, E. YONEHARA, X. DING, M. NAGAI, T. UMEGAKI and M. MATSUDA, *Biomed. Mater. Res.* **43** (1998) 46
4. K. van DIJK, H. G. SCHAEKEN, J. G. G. WOLKE and J. A. JANSE, *Biomaterials* **17** (1996) 405
5. C. K. WANG, J. H. CHEN LIN, C. P. JU, H. C. ONG and R. P. H. CHANG, *Biomaterials* **18** (1997) 1331
6. K. A. KHOR, Y. W. GU, C. H. QUEK and P. CHEANG, *Surf. Coat. Tech.* **168** (2003) 195
7. T. HANAWA, Y. KAMIURA, S. YAMAMOTO, T. KOHGO, A. AMEMIYA, H. UKAI, K. MURAKAMI and K. ASAOKA, *J. Biomed. Mater. Res.* **36** (1997) 131
8. T. HANAWA, H. UKAI and K. MURAKAMI, *J. Electron Specctrosc. Relat. Phenom.* **63** (1993) 347
9. D. KRUPA, J. BASZKIEWICZ, J. A KOZUBOWSKI, A. BARCZ, J. W. SOBCZAK, A. BILINSKI, M. LEWANDOWSKA-SZUMIEL and B. RAJCHEL, *Biomaterials* **22** (2001) 2139
10. N. OHTSU, K. SATO, K. SAITO, T. HANAWA and K. ASAMI, *Mater. Trans.* **45** (2004) 1778
11. J. H. SCOFIELD, *J. Electron Spectrosc. Relat. Phenom.* **8** (1973) 129
12. N. OHTSU, T. ASHINO and K. ASAMI, *Mater. Trans.* **45** (2004) 550
13. S. KACIULIS, G. MATTOGNO, A. NAPOLI, E. BEMPORAD, F. FERRARI, A. MONTENERO and G. GNAPPI, *J. Electron Spectrosc.* **95** (1998) 61
14. P. A. W. van der HEIDE, *Surf. Sci.* **490** (2001) L619
15. M. UCHIDA, H. M. KIM, F. MIYAJI, T. NAKAMURA and T. KOKUBO, *J. Am. Ceram. Soc.* **84** (2001) 2041

J Mater Sci: Mater Med (2007) 18:797–806
DOI 10.1007/s10856-006-0004-2

Calcium phosphate formation on titanium by low-voltage electrolytic treatments

Y. Tanaka · E. Kobayashi · S. Hiromoto · K. Asami · H. Imai · T. Hanawa

Received: 22 July 2005 / Accepted: 5 December 2005 / Published online: 2 December 2006

Abstract Electrochemical treatments are expected to be effective for the coating of calcium phosphate ceramics to a titanium substrate. In the present study, two types of chronoamperometry with a step potential and a cyclic wave potential at low voltage (up to 2.0 V) and low current density were performed in Hanks' solution to modify the surface characteristics of titanium. Titanium oxide film formed by self-passivation, that formed as reconstructed film during electrochemical treatments, and a calcium phosphate layer precipitated through treatments were characterised by X-ray photoelectron spectroscopy. The thickness and compositions of the surface films and layers were quantified from the XPS results. Calcium phosphate formation during immersion in Hanks' solution for 1.0 Ms was evaluated by scanning electron microscopy with energy-dispersive X-ray spectrometry. The results confirmed that the electrolytic treatments in this study were effective to accelerate calcium phosphate formation on titanium in Hanks' solution in spite of their lower voltage than conventional methods. The results also suggested that the hydroxyl group in the surface oxide film might contribute to the formation of calcium phosphate. This technique is a promising process for the treatment of thin titanium materials.

Y. Tanaka · E. Kobayashi (✉) · T. Hanawa
Institute of Biomaterials and Bioengineering, Tokyo Medical and Dental University, Tokyo 101-0062, Japan
e-mail: equo.met@tmd.ac.jp

Y. Tanaka · H. Imai
Department of Materials Science and Engineering, Shibaura Institute of Technology, Tokyo 108-8548, Japan

S. Hiromoto
Biomaterials Center, National Institute for Materials Science, Tsukuba 305-0044, Japan

K. Asami
Institute for Materials Research, Tohoku University, Sendai 980-8577, Japan

1 Introduction

Titanium is known to have satisfactory biocompatibility among metallic materials. Several kinds of biomedical alloys were designed till today [1–5]. To develop bone conductivity on titanium, a biomimetic ceramic coating is necessary. The mechanical properties are the result of the characteristics of the bulk structures and that biocompatibility, including bone conductivity, is the result of the surface chemical and/or physical characteristics. Applying a ceramic coating on metals is a promising method to obtain both benefits in one process. Thus, several bioceramic coating techniques, such as bioglass, AW-glass ceramics, and hydroxyapatite ($Ca_{10}(PO_4)_6(OH)_2$), have been developed [6–8].

Plasma spray coating is a well-established ceramic coating technique, and artificial hip joints made of a Ti–6Al–4V alloy coated with hydroxyapatite have been on the market for more than a decade with successful results [9]. The plasma spray coating, however, cannot be applied in sufficient amounts on complex surfaces, such as screws and porous materials. Remaining concerns are the apatite transformation that occurs during remelting at high temperatures and the flaking off of the coated layer [10]. Some other techniques to modify the surface characteristics have been reported.

Ion plating [11] and Ca ion implantation [12, 13] are effective methods, but they require the use of large facilities.

On the other hand, electrochemical treatments are commonly used to form an apatite coating on a titanium substrate. Ban and his colleagues reported on the morphology control of an apatite coating on a titanium substrate using electrolysis techniques at higher temperatures with varied currents [14, 15]. Zhu et al. succeeded in producing a Ca- and P-enriched titanium oxide film on a titanium substrate electrochemically with 70 A m^{-2} and 350 V [16]. These processes were also useful to coat a substrate with a complex surface design. Kuroda et al. used a solution containing calcium phosphate ions and hydrogen peroxide at 150 °C to coat hydroxyl apatite with different surface morphologies on a titanium substrate [17]. You et al. recently reported making a hydroxyapatite coating on dental implants with an electrophoretic technique with 20 V [18]. By these electrochemical treatments, carbonate-containing apatite with desirable morphologies, such as a plane, needles, and particles, could be precipitated on titanium. However, the processes reported above require large current, voltage, and/or higher temperatures. By applying a very large current in excess of the passive current density, the passive film on the alloys may be damaged, and active general corrosion might occur. Porous materials and thin textures will be required for future medical technologies, such as microsurgery and tissue engineering. Treatments providing biocompatibility to those materials with complex surfaces and structures will be required. A thin texture woven with thin titanium fibres is considered to be preferable as a scaffold in tissue engineering. When large current and voltage are applied, the already thin texture easily becomes thinner or dissolves by general corrosion. To avoid these outcomes, an electrolytic treatment with lower voltage is among the better solutions.

In the present study, to enhance the calcium phosphate precipitation, electrolytic treatments applying a step potential (SP) or a cyclic potential (CP) at low voltage were carried out using an artificial biofluid to modify the surface characteristics. According to previous reports, several artificial biofluids have been used for electrochemical treatments [19]. Hanks' solution was employed in this study.

An advantageous feature of this method is not to aim to maintain calcium phosphate layer with appropriate thickness on the alloy during the treatment. It is always possible that coated layers formed before implantation will flake off in clinical usage. At a lower voltage, however, this treatment provides small nuclei of precipitation distributed on the alloy surface that act as sites of natural calcium phosphate precipitation in a living body; in other words, the specks serve as sites for new bone growth. This means that the bonding of implants and bone is guaranteed by the nature of the interface between the implant surface and self-grown bone rather than by that between the implant surface and calcium phosphate coating layer formed as a result of the electrolytic treatments.

The immersion test in Hanks' solution was carried out to simulate bone formation in a living body. To evaluate calcium phosphate formation, X-ray photoelectron spectroscopy (XPS) and scanning electron microscopy (SEM) were conducted. XPS is known as a useful method to evaluate very small amounts of precipitation that are often lower than the detection limitations of SEM and energy-dispersive X-ray spectrometry (EDS). Finally, to develop a biocompatible titanium texture as a model scaffold of tissue engineering, electrolytic treatments were applied on a flatly woven titanium texture. Calcium phosphate formation on the titanium texture was also observed using SEM.

2 Experimental

2.1 Specimens and electrolytic treatments

Commercially pure titanium disks with 8 mm and 14 mm in diameter and 2.2 mm in thickness (purity 99.5 mass%) were used in the present study. Specimens were mechanically polished with SiC papers in de-ionised water and mirror-finished with diamond paste. After being washed ultrasonically in acetone, they were dried with a nitrogen gas flow.

Two kinds of electrolytic treatments using SP and CP with low voltage were developed in the present study. Hanks' solution (pH 7.4), which simulates the inorganic composition of extracellular fluid, was employed as an electrolyte for surface modification. Schematics of the treatment procedures (applied voltage) are shown in Fig. 1.

As shown in Fig. 1(a), SP was applied in one treatment. It was a typical chronoamperometry that measured the current density change while the potential increased step-like from the rest potential, E_0, to 1.0 or 2.0 V, which was a lower voltage than that in conventional methods and still in the passive state. This treatment was performed in two different durations, 1 ks and 10 ks. A potentiostat (HZ-3000, Hokuto Denko) was used to control the potential for the SP treatment. A saturated calomel electrode (SCE) was used as a reference electrode, and platinum was used as

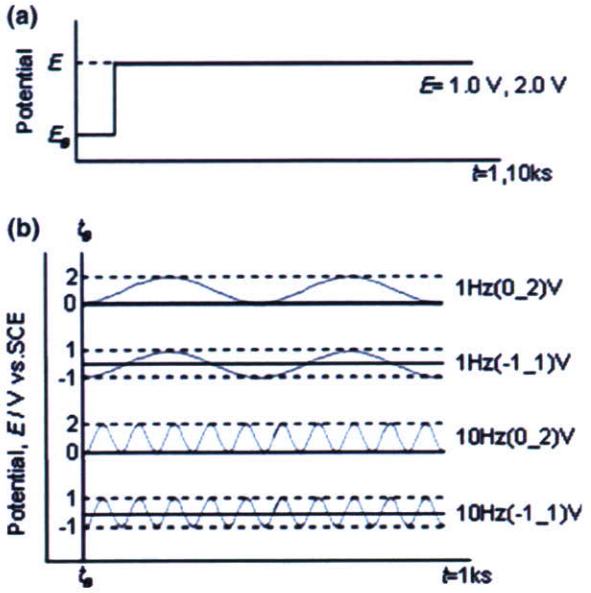

Fig. 1 Schematics of the treatment procedures showing the potential wave forms of the SP treatment (**a**) and the CP treatment (**b**)

a counter electrode. A titanium disk specimen in a Teflon holder, which was insulated from the electrolyte except for an opening window for testing, was used as a working electrode. A schematic of the working electrode is shown in Fig. 2.

In another treatment, CP with a trigonometric wave form was applied with 1 Hz or 10 Hz in frequency instead of SP, as shown in Fig. 1(b). Two different voltage waves with the same amplitude from 0 V to 2.0 V and from –1.0 V to 1.0 V were applied. For this

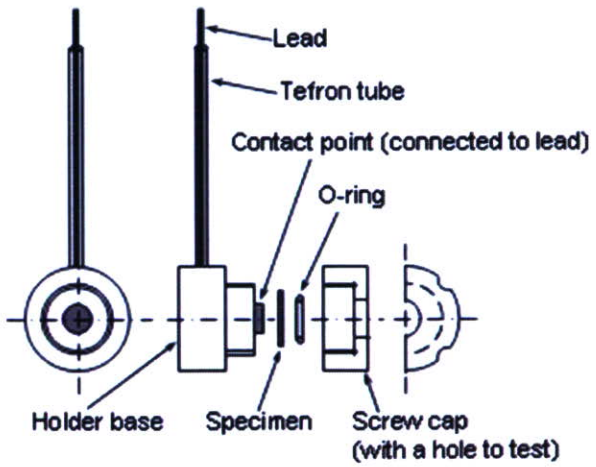

Fig. 2 Schematics of the working electrode including the specimen (titanium disk) and Teflon holder used for the SP and CP treatments. The screw cap has an opening for the test

CP treatment, a function generator (WF1946A, NF Corporation), a data acquisition system (Daq Book, Toyo Corporation), a potentiostat (HZ150G, Hokuto Denko), and data acquisition software (DASY Lab32, ADTEK System Science) to maintain the cyclic wave form were used instead of HZ–3000 in the SP treatment.

For both treatments, a test cell filled up with Hanks' solution was put in an isothermal water bath to keep the electrolyte at 310 K. The electrolyte was deaerated by high-purity nitrogen gas bubbling for 1.8 ks prior to the test.

2.2 Performance of calcium phosphate formation by immersion in Hanks' solution

To evaluate calcium phosphate formation on the surface-modified specimens, immersion in Hanks' solution was carried out after the electrolytic treatments. The specimens were immersed in Hanks' solution (42 ml) at 310 K for 1.0 Ms using sealed Teflon vessels.

2.3 XPS analysis

XPS was carried out using an X-ray photoelectron spectrometer (SSX100, SSI) in order to characterise the specimens' surface of specimens, that of after the electrolytic treatment, and that of after the electrolytic treatment and immersion in Hanks' solution. The X-ray source was monochromatised AlK_α (1486.61 eV) accelerated with 10 kV. The photoelectrons were detected through 20 eV in FAT pass energy, with a 35° take off angle.

The binding energy on the XPS spectra was corrected according to a peak binding energy of C 1s (hydrocarbon C–C and C–H) electrons at 285.0 eV due to the surface-contaminated layer [20]. The quantification of the composition and the thickness measurement of the surface films and layers were conducted with the inductive calculation method presented by Asami et al. [21], assuming stacking layers of a titanium oxide film (inner layer), a calcium phosphate layer (intermediate layer), and carbon contaminants (outer layer) on a titanium substrate.

2.4 SEM/EDS analysis

To evaluate the characteristics of calcium phosphate after immersion in Hanks' solution, SEM/EDS analysis was conducted with secondary electron images of a scanning electron microscope (JSM-5400, JEOL) at 15 kV of accelerating voltages and energy-dispersive

X-ray spectrometry (EDS) at 10 kV of accelerating voltage with 0.8 A of current density.

2.5 Electrolytic treatments on the titanium texture

In order to develop a biocompatible titanium texture, CP treatments were applied on a flatly woven titanium texture (1.0 mm in texture width, woven with eight titanium wires with a wire diameter of 0.1 mm) provided by Dr. K. Murakami of Ishikawajima-Harima Heavy Industries. Calcium phosphate formation through immersion in Hanks' solution on the titanium woven texture was observed using SEM.

3 Results

3.1 SP treatment

3.1.1 Current density response curves

The current density response curves of the SP treatments at 1.0 V for 1 ks and 10 ks are shown in Fig. 3. An inserted graph shows a close-up view of the curves within tens of seconds after the SP. The curve of the 1 ks treatment precisely overlapped with that of the 10 ks treatment even in this enlarged figure. The SP treatments at 2.0 V also showed almost identical curves. When the potential was changed from the rest potential, E_0, to a step potential (1.0 V or 2.0 V), the peak current density, I_0, appeared as the maximum value followed by steep decreasing to a very small passive current density with an asymptotic curvature. The total electric charge, Q, was calculated as a time-transient curve of the current density. For both treatment times (1 ks and 10 ks), no difference between Q and I_0 was seen because the current density had decreased asymptotically and was close to zero (in fact, it reached zero within the current resolution of the measurement system in the present study) before 1 ks. The values of I_0 and Q for each test condition are indicated in Table 1.

After these treatments, no sign of corrosion, including pitting and general corrosion, was observed.

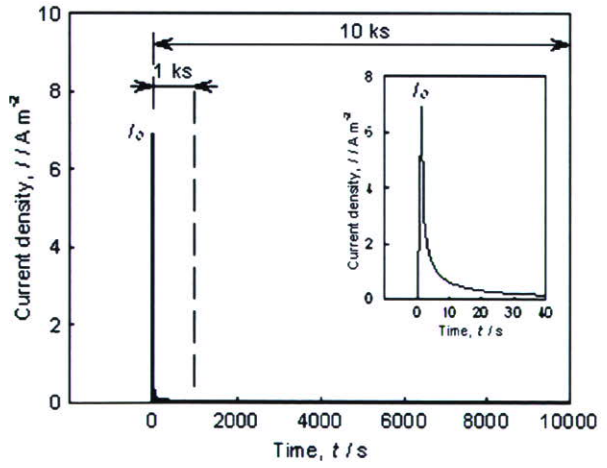

Fig. 3 Current density response curves of the SP treatments at 1.0 V for 1 ks and 10 ks showing the peak current density, I_0, and the steep decrease of the current density. An inserted graph shows a close-up view of the curves within tens of seconds after the SP

3.1.2 XPS analysis

The surfaces of SP-treated specimens exhibited a slightly golden lustre. The specimen treated at 2.0 V for 10 ks had the darkest shade of golden lustre among them. This suggested the presence of some reaction product on the film that contained yellowish ions and/or interfered with the colouring on the specimens' surface. The results of a wide range of XPS spectra are shown in Fig. 4. In the spectrum of each specimen, peaks from C, O, Ti, P, Ca, and/or N were detected.

The compositions of surface films of specimens with/without SP treatment are shown in Table 2. No Ti was detected form the specimen treated at 2 V for 10 ks, while P and Ca were detected in each specimen. This suggests that a very thick phosphate layer was formed on the titanium oxide film on the surface of the specimen treated at 2.0 V for 10 ks.

Figure 5 shows the XPS analysis of the Ti 2p electron energy region on the surfaces of all specimens. The XPS spectra were decomposed into four doublets (Ti^0, Ti^{2+}, Ti^{3+}, and Ti^{4+}) with the valence according to the binding energy reported by Asami et al. [22]. All of the specimens, other than those treated at 2.0 V for 10 ks, showed Ti $2p_{3/2}$ (higher binding energy) and Ti $2p_{1/2}$ (lower) peaks of Ti^{4+}. In addition, only the untreated specimen showed a clear spectrum peak of Ti^0, which corresponds to the metallic state. A fraction of Ti^{4+} among all Ti cations, Ti^{2+}, Ti^{3+}, and Ti^{4+}, is shown in Table 3 together with the surface film

Table 1 Results of the SP treatment for the peak current density, I_0, and the total electric charge, Q, which was calculated as a time-transient curve of the current density

	Step potential	
	1 V	2 V
I_0 (A m^{-2})	6.5	6.5
Q (C m^{-2})	3.5×10^{1}	3.7×10^{1}

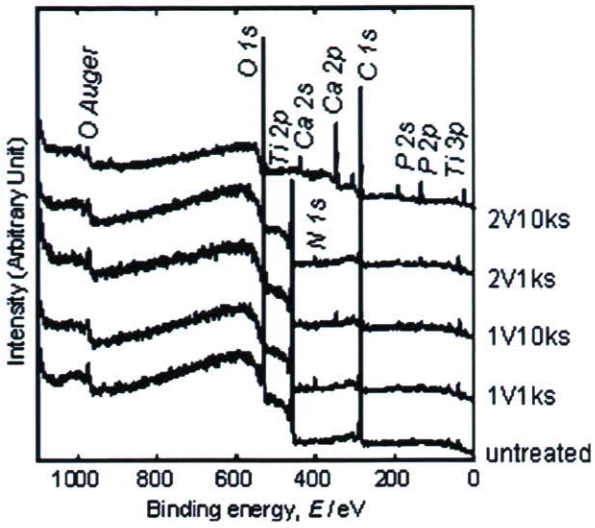

Fig. 4 Results of wide-range XPS spectra of SP-treated specimens in comparison with an untreated specimen showing C, O, Ti, P, Ca, and/or N peaks

Table 2 Compositions of the surface films of the specimens after SP treatment calculated from XPS data

	Ti	O	P	Ca
1 V–1 ks	17.19	80.79	1.63	0.38
1 V–10 ks	58.09	23.33	9.41	9.17
2 V–1 ks	18.47	79.15	2.14	0.24
2 V–10 ks	0	83.23	6.10	10.67 (mol %)

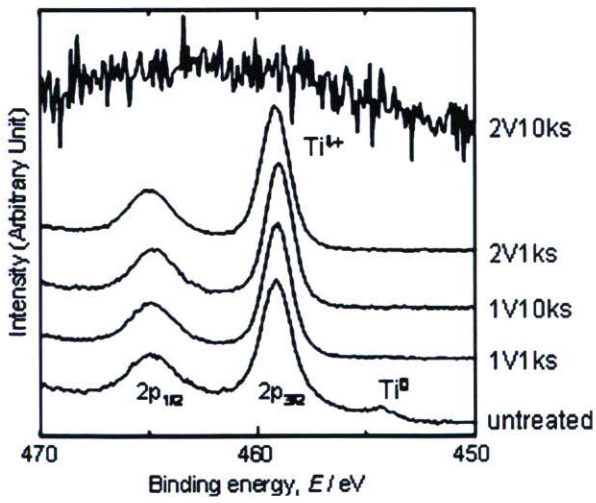

Fig. 5 Ti 2p electron energy region XPS spectra of SP-treated specimens showing Ti $2p_{3/2}$ and Ti $2p_{1/2}$ peaks of Ti^{4+}. Only the untreated specimen's spectrum showed a Ti^0 peak

thickness calculated from the XPS data. As compared to the specimen without treatment, all of the SP-treated specimens exhibited around 67% thicker surface films and an approximately 12% higher Ti^{4+} fraction. However, no significant difference in the thickness and the Ti^{4+} fraction was seen among specimens treated at 1.0 V for 1 ks, 1.0 V for 10 ks, and 2.0 V for 1 ks. The results for the specimen treated at 2.0 V for 10 ks in Tables 2 and 3 reveal that a very thick phosphate layer was formed above the titanium oxide film, which prevented the detection of any titanium cation peaks, as shown in Fig. 5.

Spectra of P 2p and Ca 2p were obtained as a set of peaks. The binding energy of P 2p electrons was 133.3–133.5 eV, while that of Ca 2p3/2 electrons was 347.3–347.6 eV in a previous study [23, 24]. According to these data, the former spectrum overlapped in the vicinity of two peaks coming from PO_4^{3-} and HPO_4^{2-}, and the latter, in the vicinity of those coming from Ca^{2+}, proving the calcium phosphate formation. The spectra of O 1s were also decomposed into three peaks of O^{2-} (oxides), OH^- (hydroxides or hydroxyl group), and H_2O (bound water or adsorbed water) [25]. The ratio of Ca and P ([Ca]/[P]) and the fraction of the OH^- in all oxygen atoms, $[OH^-]/([O^{2-}] + [OH^-] + [H_2O])$, are shown in Fig. 6. The [Ca]/[P] ratio increased in the order of 2.0 V for 10 ks: 1.0 V for 10 ks: 1.0 V for 1 ks : 2.0 V for 1 ks. These two data showed strong correspondence. The largest ratio in the specimen treated at 2.0 V for 10 ks was 1.75, which was almost identical to that of the hydroxyapatite nominal, 1.67. The same specimen showed the largest OH^- fraction, which was 0.75.

This calcium phosphate formation was reconfirmed by the SEM/EDS analysis. Figure 7 indicates the result of EDS analysis of the specimen treated at 1.0 V for 1 ks after immersion in Hanks' solution. The peaks from Ca and P, which are precipitated during immersion in Hanks' solution, are identified.

3.2 CP treatment

3.2.1 Current density response curves

The current density response curve during CP treatment at 1 Hz with –1.0 to 1.0 V is shown in Fig. 8. The maximum anodic current in each cycle of a potential wave decreased asymptotically when the testing time elapsed, while the minimum cathodic current exhibited a small fixed current around –5.0 A m^{-2}. In the case of the treatment at the same frequency with 0–2.0 V, a curve with the same tendency but drawn only in the anodic side (the minimum current was just on the

Table 3 Thickness and fraction of Ti^{4+} among all Ti cations (Ti^{2+}, $Ti3^{+}$, and Ti^{4+}) in the oxide film formed on the specimens with/without SP treatment

	Treatment conditions			
	Untreated	1 V–1 ks	1 V–10 ks	2 V–1 ks
Thickness of surface oxide (nm)	3.6	5.9	6.1	6.0
$[Ti^{4+}]/([Ti^{2+}] + [Ti^{3+}] + [Ti^{4+}])$	0.82	0.91	0.91	0.94

The thickness was calculated from XPS data according to Asami's inductive method [21]

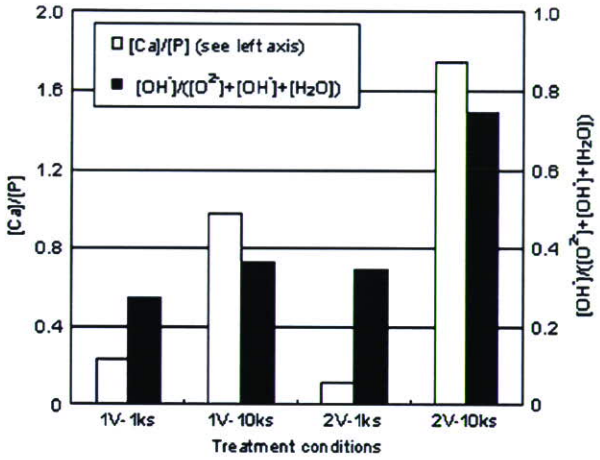

Fig. 6 Ratio of [Ca]/[P] and the fraction of the OH^- in all oxygen atoms $[OH^-]/([O^{2-}] + [OH^-] + [H_2O])$ of the surface oxide films on SP-treated specimens

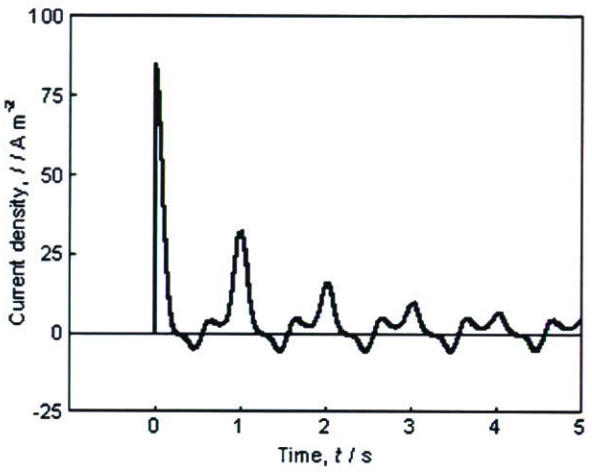

Fig. 8 Current density response curve during 1 Hz (–1_1)V CP treatment. The potential waves from were –1.0 V to 1.0 V at 1 Hz in frequency

abscissa) was obtained. For the CP treatments at 10 Hz with –1.0 to 1.0 V and 0–2.0 V, similar wave forms to 1 Hz with ten times faster frequency were seen.

No mark of pitting and general corrosion was observed in each specimen after these treatments.

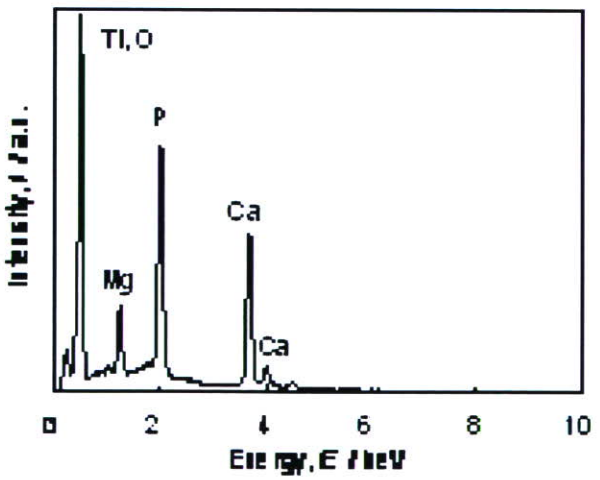

Fig. 7 SEM/EDS analysis of specimens treated at 1.0 V for 1 ks after immersion in Hanks' solution indicating peaks from Ca and P

3.2.2 *XPS analysis*

After the CP treatment, the surfaces of the specimens achieved a pale golden lustre, suggesting that the reaction products formed in the same way as with the SP treatment. The lustre was paler than that of SP-treated specimens at 2.0 V for 10 ks. Wide-range XPS analysis detected peaks from C, O, Ti, P, Ca, and/or N in each spectrum as well.

The compositions of the surface films are indicated in Table 4. In each specimen, O occupied around 80 mol % of the surface films, which was O^{2-}, OH^-, and H_2O. Specimens after CP treatment with 0–2.0 V exhibited higher Ti contents than those after CP treatment with –1.0 to 1.0 V.

The surface film thickness calculated from the XPS data and the fraction of Ti^{4+} in the oxide film are indicated in Table 5. Showing a certain correspondence between the thickness and Ti^{4+} fraction, the minimum of both data was seen in the specimen treated at 1 Hz with 0–2.0 V (4.9 nm in thickness and 0.88 in fraction), and the maximum, in the specimen at 10 Hz with 0–2.0 V (5.6 nm in thickness and 0.93 in fraction).

Table 4 Compositions of the surface films of the specimens after CP treatment calculated from XPS data

	Ti	O	P	Ca
1 Hz (0_2) V	21.19	77.56	1.01	0.13
1 Hz (–1_1) V	13.32	83.94	1.91	0.83
10 Hz (0_2) V	20.60	77.85	1.32	0.23
10 Hz (–1_1) V	18.15	78.84	1.41	1.60
				(mol %)

The spectra of P 2p and Ca 2p were also determined to come from PO_4^{3-}, HPO_4^{2-}, and Ca^{2+}, in the same way as for SP-treated specimens. The [Ca]/[P] ratio and the ratio of $[OH^-]/([O^{2-}] + [OH^-] + [H_2O])$ are shown in Fig. 9. For both the [Ca]/[P] ratio and the fraction of OH^-, the specimens treated with the potential wave from –1.0 V to 1.0 V were larger than those treated only with the anodic current (0–2.0 V). This suggests that the cathodic current might have an effect on calcium phosphate precipitation.

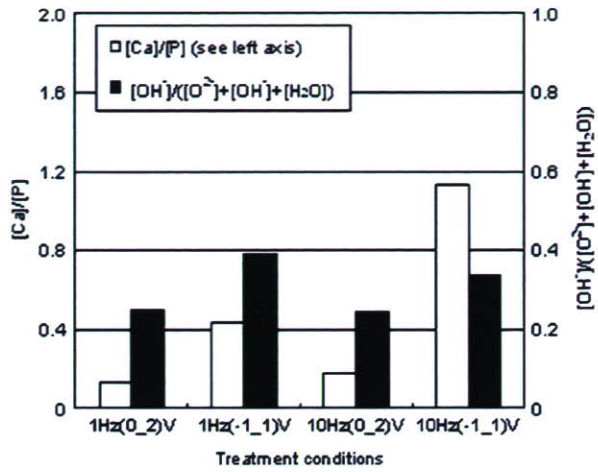

Fig. 9 Ratio of [Ca]/[P] and the fraction of the OH^- in all oxygen atoms $[OH^-]/([O^{2-}] + [OH^-] + [H_2O])$ of the surface oxide films on CP-treated specimens

3.3 Calcium phosphate formation

Figure 10 shows secondary electron images of the surface of specimens after immersion in Hanks' solution for 1.0 Ms; these images correspond to SP-treated and untreated specimens. In the EDS analysis carried out simultaneously, P, Ca, and Mg were identified in the precipitates on the surface, which suggested the formation of calcium phosphate-containing magnesium. Ban and Maruno [26] also reported that the magnesium in the calcium phosphate layer was deposited on the titanium after an electrochemical treatment using a simulated body fluid. The amount of calcium and magnesium increased proportionally to the square root of the treatment time and the cathodic potential. Comparing the SEM images, no significant difference on precipitate formation was seen between the untreated specimen and specimens treated for 1 ks. The number of calcium phosphate particles, however, obviously increased with increasing the treatment time up to 10 ks.

The results of immersion for CP-treated specimens are shown in Fig. 11. Cracks were observed in the base calcium phosphate layer formed during the CP treatment. In comparison with calcium phosphate formation during immersion, the specimens treated at –1.0 to 1.0 V showed a larger amount of precipitate.

3.4 Electrolytic treatments for titanium texture

SEM micrographs of a titanium woven texture after CP treatments at 1 Hz with –1.0 to 1.0 V followed by Hanks' solution immersion for 1.0 Ms are shown in Fig. 12. In the higher magnification on the right, calcium phosphate precipitates of around 5 μm in particle size were clearly identified with EDS. No corrosion was observed, even at higher magnification.

4 Discussion

4.1 Effects of electrolytic treatments on the surface films

The phenomenon that occurred in the electrolytic cell while the potential increased from the rest potential, E_0, to 1.0 or 2.0 V of the step potential in the SP treatment can be considered to be a charge/discharge process of the total electric charge, Q, to/from a condenser (an electric double layer) through a resistant

Table 5 Thickness and fraction of Ti^{4+} among all Ti cations in oxide film formed on the specimens after CP treatment.

	Treatment conditions			
	1 Hz(0_2) V	1 Hz (–1_1) V	10 Hz (0_2) V	1 Hz 0 (1_1) V
Thickness of surface oxide (nm)	4.9	5.3	5.6	5.1
$[Ti^{4+}]/([Ti^{2+}] + [Ti^{3+}] + [Ti^{4+}])$	0.88	0.90	0.93	0.91

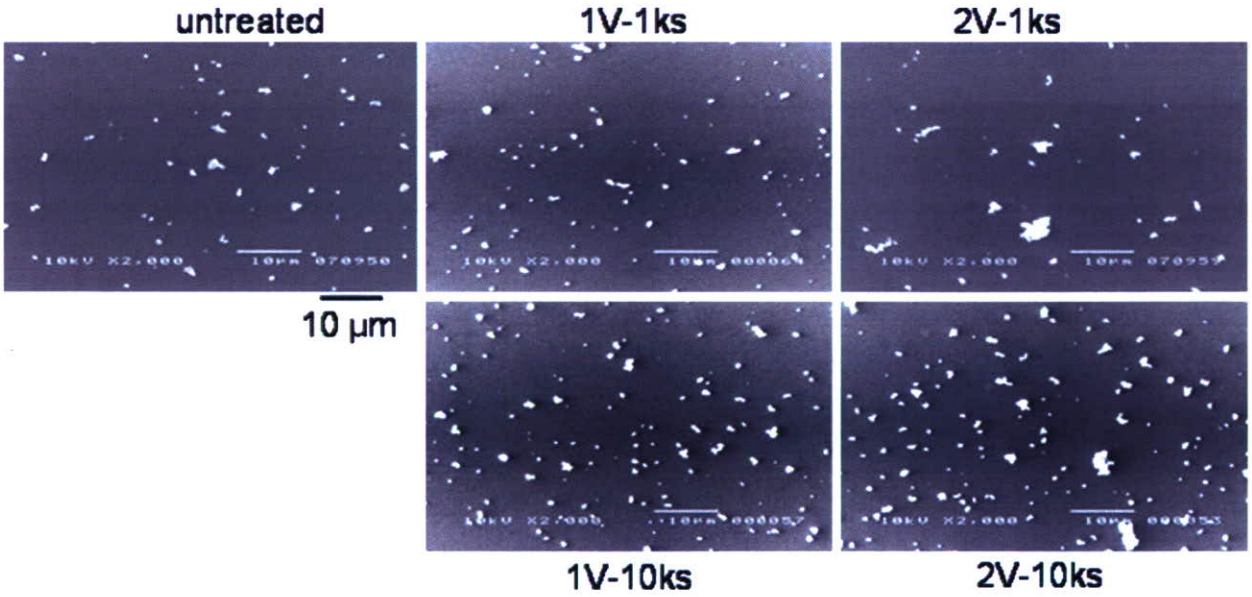

Fig. 10 SEM secondary electron images of the surface of the specimens of SP-treated and untreated specimens after immersion in Hanks' solution for 1.0 Ms, showing calcium phosphate precipitates

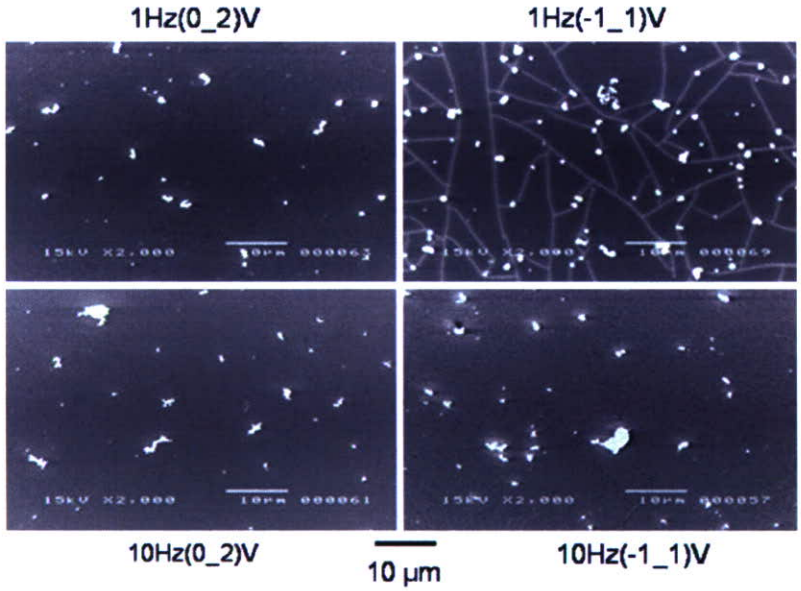

Fig. 11 SEM secondary electron images of the surfaces of specimens after CP treatment followed by immersion in Hanks' solution for 1.0 Ms. Cracks were observed in the base calcium phosphate layer on the 1 Hz(–1_1)V specimen

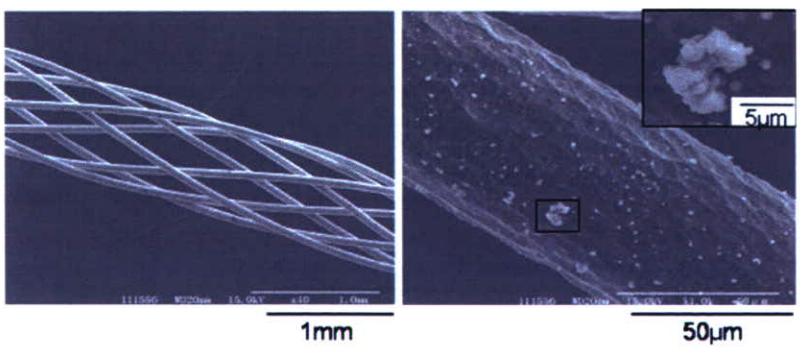

Fig. 12 SEM micrographs of a titanium woven texture after CP treatments, 1 Hz (–1_1)V, followed by immersion in Hanks' solution for 1.0 Ms. Calcium phosphate precipitates are seen in a close-up view on the right

material (Hanks' solution). The total electric charge, Q, can be calculated from the time-transient curve of the current density, and the current is controlled by the electron (ion) transfer in the testing system. When the potential is increased from the rest potential, E_0, to 1.0 V or 2.0 V, the electrons transfer from the electrolyte to the electrode. If the potential gap between the specimen and the electrolyte is larger, the electron migration becomes easier and faster just after the SP change. Then, with higher SP, the anodic current became larger. In fact, a larger total electric charge, Q, was observed at 2.0 V SP. After the electron transfer, the potential gap (including a gradient within the electric double layer) settled again in an equilibrium passive condition.

After the SP and CP treatments, the surface of titanium had a golden lustre due to the reaction product on the film that contained yellowish ions and/or showed interference colouring. The SP treatment at 2.0 V for 10 ks, which had the darkest golden lustre in the present study, was expected to have the thickest surface film formation of any treatment conditions. This thick film (layer) contained not only titanium oxide but also a certain amount of calcium phosphate [24, 27]. This means that calcium phosphate precipitation occurred during the SP treatment (before immersion in Hanks' solution) as a result of the longer treatment time.

4.2 Titanium stability in surface films

In the XPS analysis of the surfaces of the specimens after SP treatment, C, O, Ti, Ca, P, and/or N spectra were detected from the oxide films. Among them, C and N were considered to exist as a contaminated layer, and O, as oxides. Except for the SP treatment at 2.0 V for 10 ks, which exhibited no clear Ti^{4+} peaks due to the thick calcium phosphate layer, no significant difference was observed in the fraction of Ti^{4+}. Because TiO_2 is the most stable form in the titanium oxides, this Ti^{4+} fraction is considered as the stability of oxide. From these data, the SP treatment produced a thicker and more stable oxide film than that of the untreated specimen.

The thickness of the oxide film on the CP treated specimens was approximately 5 nm regardless the treatment conditions showing small difference and fraction of Ti^{4+} was varied from 88% to 93% and showed a similar tendency in thickness.

Although neither the frequency nor the different treatments, –1.0 V to 1.0 V and 0 V to 2.0 V, revealed clear effects, there was a certain correspondence between the oxide film thickness and oxide stability.

4.3 Calcium phosphate precipitation during electrolytic treatments

The fraction of OH^- among O^{2-}, OH^-, and H_2O in SP-treated specimens, as shown in Fig. 6, became larger with the treatment time. The specimens treated with 2.0 V for 10 ks showed the largest fraction of OH^-, which was larger than that of untreated specimen. The largest [Ca]/[P] ratio (1.75) was seen in the same specimen among all test conditions. For both step potentials, the very small passive current density longer than 10 ks is still effective to increase the [Ca]/[P] ratio and the OH^- fraction. Thus, the hydroxyl group might have a certain effect on the crystallinity of the calcium phosphate.

In the CP treatment at 1 Hz and 10 Hz with –1.0 V to 1.0 V, as shown in Fig. 9, the cathodic current might be a factor to form the high [Ca]/[P] ratio calcium phosphate. Moreover strong correspondence was seen between the [Ca]/[P] ratio and the hydroxyl group fraction, which suggested the hydroxyl group affected the crystallinity of the calcium phosphate in the same manner as the SP treatment. It is suggested that the cyclic exchange of anodic and cathodic currents may enhance the absorption of P and Ca alternately and that OH^- may contribute to this process.

4.4 Immersion in Hanks' solution to precipitate the calcium phosphate layer

The calcium phosphate formation of specimens SP-treated for 10 ks after immersion in Hanks' solution was comparable to that of the untreated specimen. The XPS data (no Ti^0 peak identified in specimens treated at 1.0 V for 1 ks, 1.0 V for 10 ks, 2.0 V for 1 ks and 2.0 V for 10 ks specimens) and the SEM observation suggest that the calcium phosphate precipitated not only as particles, but as a thin layer covering the surface of each specimen. The number of calcium phosphate precipitates increased with the increasing treatment time. Even though the passive current density from 1 ks to 10 ks was very small, it was still an important factor for particle precipitation and growth of the layer of the calcium phosphate. The effect of the SP difference on the precipitation was not identified within the conditions of the present study.

The immersion in Hanks' solution after CP treatment also produced both layer and particle calcium phosphate. Differently from the case of the SP treatment, cracks in the base phosphate layer on the surface treated at –1.0 V to 1.0 V were observed. These cracks were clearly caused by the thickness of the layer. However, a more detailed discussion of these cracks

and the cathodic current would exceed the scope of the present study. The number of precipitates obviously increased in the treatment at –1.0 to 1.0 V.

As stated above, both the very small passive current (in the SP treatment) and the cathodic current (in the CP treatment with –1.0 to 1.0 V) were effective to accelerate the calcium phosphate formation. Although the mechanisms in either case may differ, they have not been clearly identified. As shown in Figs. 6 and 9, the existence of the hydroxyl group shows a certain correlation to calcium phosphate formation. It is strongly suggested that the hydroxyl group affects the absorption of Ca and P ions and/or the formation of calcium phosphate on the surface. The very small passive current in the SP treatment and the cathodic current in the CP treatment might have a role in this process.

5 Conclusion

Calcium phosphate was precipitated on a titanium surface by the SP and CP treatments together with a titanium oxide film. In the SP treatment, the stability of the oxide thickness of the oxide film and the fraction of the hydroxyl group on the surface became larger with a longer treatment time. In the CP treatment, the stability of the oxide thickness of the oxide film and the fraction of the hydroxyl group on the surface became larger in the treatment with a potential wave at –1.0 to 1.0 V rather than at 0–2.0 V. The very small passive current in the SP treatment and the cathodic current in the CP treatment enhanced the calcium phosphate formation. SP and CP treatments were effective to accelerate calcium phosphate precipitation on titanium in Hank's solution in spite of their lower voltage than that of the conventional methods. The calcium phosphate formation was accelerated by the hydroxyl group in Hanks' solution.

References

1. A. K. SHUKLA, R. BALASUBRAMANIAM and S. BHARGAVA, J. Alloys Compd. **389** (2005) 144
2. E. EISENBARTH, D. VELTEN, M. MULLER, R. THULL and J. BREME, Biomaterials **25** (2004) 5705
3. J. I. QAZI, B. MARQUARDT and H. J. RACK, JOM **56** (2004) 49
4. M. TAKAHASHI, E. KOBAYASHI, H. DOI, T. YONEYAMA and H. HAMANAKA, J. Jpn Inst. Metals **64** (2000) 1120
5. E. KOBAYASHI, H. DOI, T. YONEYAMA, H. HAMANAKA, I. R. GIBSON, S. M. BEST, J. C. SHELTON and W. BONFIELD, J. Mater. Sci. Mater. Med. **9** (1998) 625
6. T. KITSUGI, T. NAKAMURA, M. OKA, Y. SENAHA, T. GOTO and T. SHIBUYA, J. Biomed. Mater. Res. **30** (1996) 261
7. V. A. DUBOK, *Powder Metall. Met. Ceram.* **39** (2000) 381
8. L. M. SUN, C. C. BERNDT, K. A. GROSS and A. KUCUK, J. Biomed. Mater. Res. **58** (2001) 570
9. W. J. A. DHERT, Med. Prog. Technol. **20** (1994) 143
10. M. FINI, A. CIGADA, G. RONDELLI, R. CHIESA, R. GIARDINO, G. GIAVARESI, N. N. ALDINI, P. TORRICELLI and B. VICENTINI, Biomaterials **20** (1999) 1587
11. M. YOSHINARI, Y. OHTSUKA and T. DERAND, Biomaterials **15** (1994) 529
12. T. HANAWA, Y. NODASAKA, H. UKAI, K. MURAKAMI and K. ASAOKA, J. Jpn Soc. Biomater. **12** (1994) 209
13. T. HANAWA, Y. KAMIURA, S. YAMAMOTO, T. KOHGO, A. AMEMIYA, H. UKAI, K. MURAKAMI and K. ASAOKA, J. Biomed. Mater. Res. **36** (1997) 131
14. S. BAN and S. MARUNO, Biomaterials **19** (1998) 1245
15. S. BAN and J. HASEGAWA, Biomaterials **23** (2002) 2965
16. X. L. ZHU, K. H. KIM and Y. S. JEONG, Biomaterials **22** (2001) 2199
17. K. KURODA, Y. MIYASHITA, R. ICHINO and M. OKIDO, Mater. Sci. Forum **426–4** (2003) 3189
18. C. K. YOU, X. W. MENG, T. Y. KWON, Y. Z. YANG, J. L. ONG, S. KIM and K. H. KIM, Bioceramics **17** (2005) 901
19. T. HANAWA, K. ASAMI and K. ASAOKA, J. Biomed. Mater. Res. **40** (1998) 530
20. K. ASAMI, J. Electr. Spectrosc. **9** (1976) 469
21. K. ASAMI, K. HASHIMOTO and S. SHIMODAIRA, Corros. Sci. **17** (1977) 713
22. K. ASAMI, S. C. CHEN, H. HABAZAKI and K. HASHIMOTO, Corros. Sci. **35** (1993) 43
23. T. HANAWA and M. OTA, Biomaterials **12** (1991) 767
24. T. HANAWA and M. OTA, Appl. Surf. Sci. **55** (1992) 269
25. K. ASAMI and K. HASHIMOTO, Corros. Sci. **17** (1977) 559
26. S. BAN and S. MARUNO, Jpn J. Appl. Phys. **32** (1993) L1577
27. K. E. HEALY and P. DUCHEYNE, J. Biomed. Mater. Res. **26** (1992) 319

Structure and strength at the bonding interface of a titanium-segmented polyurethane composite through 3-(trimethoxysilyl) propyl methacrylate for artificial organs

Harumi Sakamoto,[1] Hisashi Doi,[1] Equo Kobayashi,[1] Takayuki Yoneyama,[1] Yoshiaki Suzuki,[2] Takao Hanawa[1]

[1]*Department of Metallurgy, Institute of Biomaterials and Bioengineering, Tokyo Medical and Dental University, Tokyo 101-0062, Japan*

[2]*Beam Application Team, Advanced Development and Supporting Center, RIKEN, Wako 351-0198, Japan*

Received 14 March 2006; revised 19 April 2006; accepted 8 June 2006
Published online 31 January 2007 in Wiley InterScience (www.interscience.wiley.com). DOI: 10.1002/jbm.a.30957

Abstract: The objective of this study was to investigate the structure and strength at the bonding interface of a titanium (Ti)-segmented polyurethane (SPU) composite through (3-trimethoxysilyl) propyl methacrylate (γ-MPS) for artificial organs. The effects of the thickness of the γ-MPS layer on the shear bonding strength between Ti and SPU were investigated. Ti disks were immersed in various concentrations of γ-MPS solutions for several immersion times. The depth profiles of elements and the thickness of the γ-MPS layer were determined by glow discharge optical emission spectroscopy and ellipsometry, respectively. The bonding stress at the Ti/γ-MPS/SPU interface was evaluated with a shear bonding test. Furthermore, the fractured surface of a Ti-SPU composite was observed by optical microscopy and characterized using X-ray photoelectron spectroscopy. Consequently, the thickness of the γ-MPS layer was controlled by the concentration of the γ-MPS solution and immersion time. The shear bonding stress at the interface increased with the increase of the thickness of the γ-MPS layer. Therefore, the control of the thickness of the γ-MPS layer is significant to increase the shear bonding stress at the Ti/γ-MPS/SPU interface. These results are significant to create composites for artificial organs consisting of other metals and polymers. © 2007 Wiley Periodicals, Inc. J Biomed Mater Res 82A: 52–61, 2007

Key words: titanium; segmented polyurethane; silane coupling agent; shear bonding stress; surface analysis

INTRODUCTION

Polymers are widely used as biomaterials because of their high degree of flexibility, biocompatibility, and technological properties.[1–4] For example, polyurethane and polyacrylonitrile are used as blood vessel prostheses and artificial kidneys, respectively. Segmented polyurethane (SPU) is also widely used because of its antithrombogenicity.[2,5,6] In addition, since the biofunctionalization of the polymer surface by surface modification is easy, it has been undertaken to improve biocompatibility.[7] To maintain an antithrombogenic surface for artificial vessels, a poly(ethylene glycol) or 2-methacryloyloxyethyl phosphorylcholine polymer has been immobilized to the polymer surfaces in the previous studies.[8,9] However, the polymers show insufficient strength and long-term durability for some purposes because of their structures. Thus, the improvement of the strength and durability of the polymers is sometimes required.

On the other hand, metals have been used widely as biomaterials (for stents, hip joints, and bone plates) for a long time, since metals have good mechanical properties, especially toughness, and long-term durability.[1] In particular, titanium (Ti) and Ti alloys are the most promising metallic biomaterials because of their high corrosion resistance and tissue compatibility among metals. However, the biocompatibility of metals is generally inferior to that of polymers and ceramics because no biofunction is added to the metals during the manufacturing process.

If a polymer and a metal could be bonded and used as a composite material, a new material having good biocompatibility and high mechanical strength could be created. The interfacial chemical structure governing the bonding strength, especially at the

Correspondence to: T. Hanawa; e-mail: hanawa.met@tmd.ac.jp

Contract grant sponsor: Japanese Society for Artificial Organs (JSAO)-Grant 2005

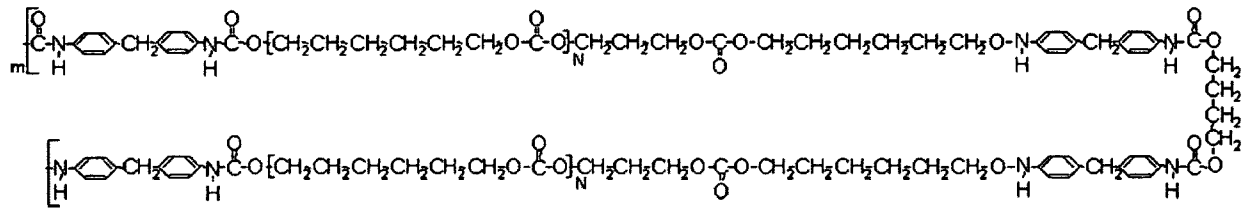

Figure 1. Chemical structure of corehtane70A.

nanometer level, is one of the most challenging aspects to the development of composite materials.

The bonding of polymers with metals is currently utilized in dentistry.[10–14] Investigators have tried to combine a Ti alloy and a resin for crown facings.[15] In particular, silane coupling agents containing S—H groups and Si—O—CH_3 groups are comprehensively used to combine dental alloys with resins.[16] The S—H groups works as a bonding agent with polymers; the Si—O—CH_3 works as a bonding agent with metals. The mechanical properties and durability of composite resin increases with silanized filler.[17–21] However, in most studies about materials using silane coupling agents in the field of dentistry, only the bonding strength is evaluated and discussed, and there are few reports that examine and discuss the chemical structures at the bonding interface and how they influence the bonding strength.

Other studies on silane coupling agents to combine polymers with metals have been performed in other fields. An aluminum–vegetable oil composite using a silane coupling agent has been developed.[22,23] Rubber-to-metal bonding by a silane coupling agent was investigated.[24] In addition, the surface modification of stainless steel by grafting of poly(ethylene glycol) using a silane coupling agent has been reported.[25] However, only the chemical structure is investigated in these studies. In other words, the relationship between the bonding strength and the interfacial chemical structure containing a silane coupling agent layer has not been studied.

The objective of this study was to investigate the unequivocal relationship between the shear bonding strength and the chemical structure at the bonding interface of a metal–polymer composite through a silane coupling agent. As the base materials for the composite, Ti and SPU were used, the shear bonding strength between Ti and SPU of Ti-SPU composites manufactured under various bonding conditions was evaluated. Furthermore, the nanometer-level structures at the interface and the fractured surface of the composite were investigated. From these results, factors that affect the bonding strength were specified. It is our hope that this study will lead to enhancements in the creation of metal–polymer composites for artificial organs.

MATERIALS AND METHODS

Specimen preparation

Commercially pure Ti disks with 2 and 5 mm in thickness and 8 mm in diameter were prepared from wrought titanium rods (grade 2; Rare Metallic, Japan). The disks were polished with a 320 and 600 grid SiC papers in water, followed by buffing with 9-μm size diamond paste and a 0.05-μm size alumina slurry for a mirror-finished surface. The disks were ultrasonically rinsed in acetone and deionized water for 5 min. The surface of the 2-mm thick disks was characterized using X-ray photoelectron spectroscopy (XPS). The detail of XPS analysis is described later. Solutions of 0.1, 0.5, 1.0, and 2.0vol% 3-(trimethoxysilyl) propyl methacrylate (γ-MPS) were prepared by diluting 100%-concentration γ-MPS (Kanto Chemical, Japan) with deionized water and adjusted at pH 4 using acetic acid. These solutions were then hydrolyzed for 1 h under stirring and filtered using a 40-μm membrane filter. Prior to the γ-MPS coating, both 2- and 5-mm thick disks were ultrasonically cleaned again in acetone for 5 min. The cleaned disks were then immersed in the freshly prepared γ-MPS solutions for 1, 10, 50, and 100 min. The disks were dried with a stream of high-purity nitrogen gas and kept in a vacuum desiccator.

The depth profiles of elements and the thickness of the γ-MPS layer deposited on 2-mm thick disks were determined by glow discharge optical emission spectroscopy (GD-OES) and ellipsometry, respectively, whereas 5-mm thick disks coated with the γ-MPS layer were used for a shear bonding test. To prepare a 3.0vol% SPU solution, 600 mg Corehtane70A (Crovita) with the chemical structure shown in Figure 1, 10-mL tetrahydrofuran (Kanto Chemical), and 10-mL dimethylformamide (Kanto Chemical) were mixed. Ti disks coated with the γ-MPS layer were then immersed in the freshly prepared SPU solution and kept in the vacuum desiccator for 2 days. Thereafter, the Ti-SPU composites were removed from the SPU solution and dried in the vacuum desiccator again. The grip for the shear bonding test was thus formed on the surface of the SPU layer using an autopolymerized acrylic resin (UNIFAST II, GC, Japan). Fractured surface was characterized using XPS. The flowchart of the experimental procedure is shown in Figure 2. The γ-MPS concentration and immersion time of specimens used for GD-OES, ellipsometry, shear bonding tests, and XPS are summarized in Table I.